5170 *Chem. Mater.* **2009,** *21,* 5170–5175
DOI:10.1021/cm9021134

CHEMISTRY OF MATERIALS
Article

Synthesis of Ultrathin Hexagonal Palladium Nanosheets

Prem F. Siril,[†,⊥] Laurence Ramos,[‡] Patricia Beaunier,[§] Pierre Archirel,[†] Arnaud Etcheberry,[∥] and Hynd Remita*[,†]

[†]*Laboratoire de Chimie Physique, UMR 8000-CNRS, Université Paris-Sud 11, 91405 Orsay, France,* [‡]*Laboratoire des Colloïdes, Verres et Nanomatériaux, UMR 5587-CNRS, Université Montpellier II, 34095 Montpellier Cedex 05, France,* [§]*Laboratoire de Réactivité de Surface, UMR 7197-CNRS, Université Paris-VI, 75252 Paris Cedex 05, France, and* [∥]*Institut Lavoisier de Versailles, ILV UMR 8180-CNRS, Université Versailles Saint-Quentin-en-Yvelines, 45 rue des Etats-Unis, 78035 Versailles Cedex, France.* [⊥]*Present address: Chemistry Department, National Institute of Technology, Hamirpur-177 005, Himachal Pradesh, India.*

Received July 13, 2009. Revised Manuscript Received September 23, 2009

Ultrathin palladium hexagonal nanosheets were synthesized in emulsions constituted of droplets of toluene containing Pd complexes in water and stabilized by CTAB as surfactant and in quaternary mesophases formed by water, toluene containing Pd complexes, CTAB, and a cosurfactant. We have identified slow reduction and nucleation provided by CO and adsorption at the CTAB interface as key factors for the formation of Pd nanosheets. These nanosheets exhibit a broad absorption band from the visible to the near-infrared region.

I. Introduction

Nanomaterials often exhibit remarkable properties when compared to bulk materials.[1] Exceptional magnetic,[2] optical,[3] electronic,[4] and catalytic[5] properties can be exploited for numerous technological applications. Properties such as catalytic and electrocatalytic activities could strongly depend on the size and shape of the metal nanoparticles.[6] Therefore synthesis of nanoparticles that could exhibit well-controlled shapes and sizes has been explored to enhance their performances.[7]

Pd is a versatile catalyst for a large number of industrially important reactions such as hydrogenation of unsaturated organic compounds[6d,8] and a number of important C−C coupling reactions.[9] Pd is also a performing material for hydrogen storage and sensing.[10] Pd nanoparticles show high catalytic activity for ethanol electrooxidation in basic media, and its electroactivity is even higher than that of Pt.[11]

Pd nanoparticles with different shapes have been synthesized by controlled growth on specific crystallographic faces or by templating methods. Xia et al. have recently published a review on the shape controlled synthesis of Pd nanocrystals in aqueous solutions.[12] Triangular and hexagonal nanoplates obtained by a polyol process exhibit interesting surface plasmon resonance and surface enhanced Raman scattering (SERS).[13] Rectangular Pd particles were prepared at room temperature by using cetyltrimethylammonium bromide (CTAB) as a surfactant.[14] Single crystalline Pd nanothorns were prepared with a square wave electrochemical reduction method, without any template or surfactant.[15] Highly

*Corresponding author. E-mail: hynd.remita@lcp.u-psud.fr.

(1) Rao, C.N. R.; Muller, A.; Cheetham, A. K., Eds. *The Chemistry of Nanomaterials: Synthesis, Properties and Applications*; Wiley-VCH Verlag GmbH & Co. KgaA: Weinheim, **2004**.
(2) (a) Punter, V. F.; Krishnan, K. M.; Alivistaos, A. P. *Science* **2001**, *291*, 2115. (b) Sun, S.; Murray, C. B.; Weller, D.; Folks, L.; Moses, A. *Science* **2000**, *287*, 1989.
(3) Eychmuller, A. *J. Phys. Chem. B* **2001**, *104*, 6514.
(4) Huynh, W. U.; Dittmer, J. J.; Alivisatos, A. P. *Science* **2002**, *295*, 2425.
(5) El-Sayed, M. A. *Acc. Chem. Res.* **2001**, *34*, 257.
(6) (a) Sasaki, M.; Osada, M.; Higashimoto, N.; Yamamoto, T.; Fukuoka, A; Ichikawa, M. *J. Molec. Catal. A: Chem.* **1999**, *141*, 223. (b) Narayanan, R.; El-Sayed, M. A. *Nano Lett.* **2004**, *4*, 1343. (c) Wang, C.; Daimon, H.; Lee, Y.; Kim, J.; Sun, S. *J. Am. Chem. Soc.* **2007**, *129*, 6974. (d) Berhault, G.; Bisson, L.; Thomazeau, C.; Verdon, C.; Uzio, D. *Appl. Catal. A* **2007**, *327*, 32. (e) Ahmadi, T. S.; Wang, Z. L.; Green, T. C.; Henglein, A.; El-Sayed, M. A. *Science* **1996**, *272*, 1924. (f) Xiong, Y.; Xia, Y. *Adv. Mater.* **2007**, *19*, 3385.
(7) (a) Kuhn, J. N.; Huang, W.; Tsung, C. K.; Zhang, Y.; Somorjai, G. A. *J. Am. Chem. Soc.* **2008**, *130*, 14026. (b) Fukuoka, A.; Higashimoto, N.; Sakamoto, Y.; Inagaki, S.; Fukushima, Y.; Ichikawa, M. *Microporous Mesoporous Mater.* **2001**, *48*, 171.
(8) Redjala, T.; Remita, H.; Apostolescu, G.; Mostafavi, M.; Thomazeau, C.; Uzio, D. *Gas Oil Sci. Technol.* **2006**, *61*, 789.
(9) (a) Li, Y.; Hong, X. M.; Collard, D. M.; El-Sayed, M. A. *Org. Lett.* **2000**, *2*, 2385. (b) Reetz, M. T.; Westermann, E. *Angew. Chem., Int. Ed.* **2000**, *39*, 165. (c) Astruc, D. *Inorg. Chem.* **2007**, *46*, 1884. (d) Franze, R. *Can. J. Chem.* **2000**, *78*, 957. (e) Son, S. U.; Jang, Y.; Park, J.; Na, H. B.; Park, H. M.; Yun, H. J.; Lee, J.; Hyeon, T. *J. Am. Chem. Soc.* **2004**, *126*, 5026.
(10) (a) Tobiska, P.; Hugaon, O.; Trouillet, A.; Gagnaire, H. *Sens. Actuators, A* **2001**, *74*, 168. (b) Favier, F.; Walter, E. C.; Zach, M. P.; Benter, T.; Penner, R. M. *Science* **2001**, *293*, 2227. (c) Langhammer, C.; Zoric, I.; Kasemo, B. *Nano Lett.* **2007**, *7*, 1343.
(11) (a) Gupta, S. S.; Datta, J. *J. Power Sources* **2005**, *145*, 124. (b) Liu, J.; Ye, J.; Xu, C.; Jiang, S. P.; Tong, Y. *Electrochem. Commun.* **2007**, *9*, 2334. (c) Xu, C.; Wang, H.; Shen, P. K.; Jiang, S. P. *Adv. Mater.* **2007**, *19*, 4256. (d) Mackiewicz, N.; Surendran, G.; Remita, H.; Keita, B.; Zhang, G.; Nadjo, L.; Hagege, A.; Doris, E.; Mioskowski, C. *J. Am. Chem. Soc.* **2008**, *130*, 8110.
(12) Lim, B.; Jiang, M.; Tao, J.; Camargo, P. H. C.; Zhu, Y.; Xia, Y. *Adv. Funct. Mater.* **2009**, *19*, 189.
(13) Xiong, Y.; McLellan, J. M.; Chen, J.; Yin, Y.; Li, Z. Y.; Xia, Y. *J. Am. Chem. Soc.* **2005**, *127*, 17118.
(14) Sun, Y.; Zhang, L.; Zhou, H.; Zhu, Y.; Sutter, E.; Ji, Y.; Rafailovich, M. H.; Sokolov, J. C. *Chem. Mater.* **2007**, *19*, 2065.
(15) Meng, H.; Sun, S.; Masse, J. P.; Dodelet, J. P. *Chem. Mater.* **2008**, *20*, 6998.

 Published on Web 10/07/2009

ordered Pd nanowire arrays were prepared by electrodeposition using anodized aluminum oxide as template, and these arrays were found to be very active catalysts for ethanol oxidation for direct alcohol fuel cells.[11c] Nanostructured Pd particles such as nanocubes, nanotetrahedra, nanopolyhedra, and nanorods were prepared using a seed-mediating approach in the presence of CTAB.[6d,16] Self-assembled Pd nanosheets were prepared from organic medium using a layered organic−inorganic hybrid composite as template.[17] Porous Pd nanoballs[18] and nanowires[19] were recently synthesized using hexagonal mesophases as templates. Flower-like nanostructures, foils, hexagonal nanoplates, and nanowires were obtained by radiolysis or photoreduction in 2-propanol under CO atmosphere.[20] Controlling the shape of Pd nanostructures is not only important in enhancing the catalytic activity but also for other applications such as SERS[13,21] and optical sensing.[22] Additionally it has been reported that two-dimensional Pd nanoparticles show ferromagnetic properties that differ from those of bulk Pd.[23] A recent study also indicated that the Pd nanoplatelets have greater capacity for hydrogen absorption than bulk Pd and spherical Pd nanoparticles.[24]

We present here the synthesis of hexagonal Pd nanosheets in ternary emulsions made of water/oil/surfactant and quaternary hexagonal mesophases made of water/oil/surfactant/cosurfactant. These nanostructures exhibit a broad absorption band from the visible to the near-infrared region.

II. Experimental Section

Materials. All the high purity chemicals such as cetyltrimethylammonium bromide CTAB, sodium dodecylsulfate SDS, tris-(benzylidum)dipalladium (0) $Pd_2(DBA)_3$, palladium acetate $Pd^{II}(OAc)_2$, palladium acetylacetonate $Pd^{II}(acac)_2$, toluene, NaCl, 2-propanol, and 1-pentanol were purchased from Sigma-Aldrich and were used as received. The CO was purchased from Air Liquide.

Sample Preparation. *Preparation of the Emulsions*. A total of 2.06 g of CTAB (or 1.6 g SDS) was first dissolved in 4 mL of a 0.1 M NaCl aqueous solution at 50 °C in pyrex glass tubes to get a transparent, viscous micellar solution. In both cases, the surfactant concentration is fixed at 1.38 M. On the other hand, the Pd precursors complexes, $Pd_2(DBA)_3$, $Pd(OAc)_2$, or $Pd(acac)_2$), were dissolved in toluene at a concentration of 1.5×10^{-3} M. The solutions containing $Pd_2(DBA)_3$ are red while those containing $Pd(OAc)_2$ or $Pd(acac)_2$ are yellow. A total of 6 mL of the solution of Pd precursors in toluene was added to the pristine micellar solution. The mixture was vortexed thoroughly to form a yellow orange emulsion, for CTAB-based samples, and a red wine emulsion, for SDS-based samples.

A more dilute CTAB-based emulsion with $Pd_2(DBA)_3$ was also prepared in a similar manner but with 8 mL of aqueous solution of NaCl (0.1 M) instead of 4 mL. A pale yellow colored emulsion was formed.

The emulsion consists of oil droplets of micrometer size stabilized by surfactant molecules in brine.

Preparation of the Mesophases. The hexagonal mesophases with CTAB as surfactant were prepared following the previously published method with some modifications.[18,19,25] Typically, 2.06 g of CTAB was first dissolved in 4 mL of brine (0.1 M) at 50 °C in pyrex glass tubes. A total of 6 mL of $Pd_2(DBA)_3$, $Pd(OAc)_2$, or $Pd(acac)_2$ solution in toluene (1.5×10^{-3} M) was added to this micellar solution and vortexed strongly to form an opaque gel that on further mixing with a few drops of 1-pentanol (40 μL) yielded a transparent, gelatinous, yellow orange mesophase. A CTAB-based mesophase with higher $Pd(OAc)_2$ concentration (10^{-2} M) was also prepared. At higher $Pd(OAc)_2$ concentration, the mesophase is orange. The mesophases thus prepared were kept sealed and allowed to equilibrate for a few days before use for further experiments. Other hexagonal mesophases doped with $Pd_2(DBA)_3$ and produced with SDS as surfactant were prepared similarly. The obtained mesophases were wine red colored.

The mesophases are swollen hexagonal phases, which are constituted of infinitely long surfactant-stabilized oil tubes that are regularly arranged in brine. The center-to-center distance between adjacent tubes in the hexagonal mesophases and the diameter of the tubes are respectively of the order of 20 nm and 18 nm, as determined by small-angle X-ray scattering (data not shown).

Experiments conducted with mesophases of another symmetry (lamellar phase obtained with slightly larger quantity of pentanol than for hexagonal mesophases) gave similar results.

Preparation of the Pd Nanostructures. Pd nanostructures were prepared by passing CO through the samples. Typically, a small amount of sample was carefully transferred to a small pyrex bottle (10 mL) and sealed with a rubber septum. The sample was flushed by flowing Argon, and then CO (1 atm) was carefully passed through the sample at a very low flow rate for 15 min. As CO is very toxic, the bubbling was done in a very well ventilated hood with external evacuation. CO diffuses very slowly into the sample, and the reaction of CO with $Pd_2(DBA)_3$ (or the other Pd complexes) causes the color change from yellow orange to blue (in the case of CTAB-based samples) or from red to black (in case of SDS-based samples). The Pd nanomaterials were extracted by addition of 2-propanol, centrifuged, and washed several times with 2-propanol under ultrasonication to remove the surfactant.

Characterization Techniques. The UV−visible spectra were recorded on a double beam Perkin-Elmer Lambda 19 spectrophotometer.

A dilute dispersion of the purified nanostructures in 2-propanol was sonicated for a few minutes to disperse the Pd nanomaterials. This solution was dropped over a carbon-coated copper grid and dried under air for transmission electron

(16) Berhault, G.; Bausach, M.; Bisson, L.; Becerra, L.; Thomazeau, C.; Uzio, D. *J. Phys. Chem. C* **2007**, *111*, 5915.
(17) Cheng, Z.; Pan, D.; Wang, H.; Pang, M.; Han, Y.; Lin, J. *Nanotechnology* **2006**, *17*, 506.
(18) Surendran, G.; Ksar, F.; Ramos, L.; Keita, B.; Nadjo, L.; Prouzet, E.; Beaunier, P.; Audonnet, F.; Remita, H. *J. Phys. Chem. C* **2008**, *112*, 10740.
(19) Ksar, F.; Surendran, G.; Ramos, L.; Keita, B.; Nadjo, L.; Prouzet, E.; Beaunier, P.; Hagege, A.; Audonnet, F.; Remita, H. *Chem. Mater.* **2009**, *21*, 1612.
(20) Redjala, T.; Apostolescu, G.; Beaunier, P.; Mostafavi, M.; Etcheberry, A.; Uzio, D.; Thomazeau, T.; Remita, H. *New J. Chem.* **2008**, *32*, 1403.
(21) Li, Y.; Lu, G.; Wu, X.; Shi, G. *J. Phys. Chem. B* **2006**, *110*, 24585.
(22) Langammer, C.; Zoric, I.; Kasemo, B. *Nano Lett.* **2007**, *7*, 3122.
(23) (a) Bouarab, S.; Damangeat, C.; Mokrani, A.; Dreysse, H. *Phys. Lett. A* **1990**, *151*, 103. (b) Suzuki, M.; Suzuki, I. S.; Walter, J. *Phys. Rev. B* **2000**, *62*, 14171. (c) Mendoza, D.; Morales, F.; Escundero, E.; Walter, J. *J. Phys.: Condens. Mater* **1999**, *11*, L317.
(24) Kishore, S.; Nelson, J. A.; Adair, J. H.; Eklund, P. C. *J. Alloys Compd.* **2005**, *389*, 234.
(25) Surendran, G.; Pena dos Santos, E.; Tokumoto, M. S.; Remita, H.; Ramos, L.; Kooyman, P. J.; Santilly, C. S.; Bourgaux, C.; Dieudonné, P.; Prouzet, E. *Chem. Mater.* **2005**, *17*, 1505.

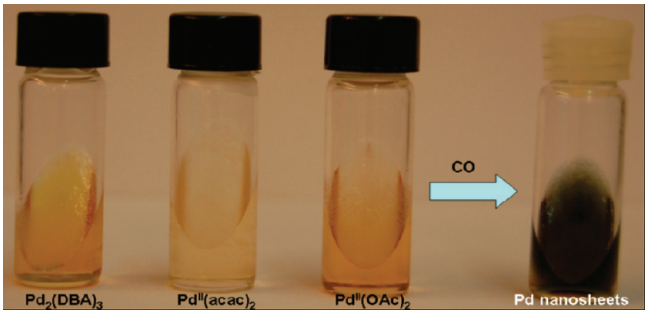

Figure 1. CTAB-based hexagonal mesophases containing Pd complexes (1.5×10^{-3} M in the oil phase) before and after the reaction with CO.

microscopy (TEM) imaging with a JEOL 100 CXII instrument at an accelerating voltage of 100 kV. High resolution TEM imaging was performed on a JEOL JEM 2010 equipped with a LaB_6 filament operating at 200 kV. The images were collected with a 4008 × 2672 pixels CCD camera (Gatan Orius SC1000).

The X-ray photoelectron spectroscopy (XPS) analysis was performed on InP foils. Sample drops were deposited on the foils and dried under Argon flow. The XPS analyzer was a Thermo Electron ESCALAB 220i-XL. Either a nonmonochromatic or a monochromatic X-ray Al Kα line was used for excitation. The photoelectrons were detected perpendicularly to the support. A constant analyzer energy mode was used with pass energy of 20 eV.

III. Results and Discussion

Upon reaction with CO, the initially yellow orange CTAB-based emulsions containing $Pd_2(DBA)_3$ turn to a blue color. The same change of color from orange to blue had also occurred with CTAB-based hexagonal mesophases (Figure 1).

The Pd nanostructures synthesized in CTAB-based emulsions or mesophases doped with different Pd complexes were extracted with 2-propanol. The TEM pictures show Pd nanosheets without well-defined shapes (Figure 2a). After washing several times to remove the surfactant, the TEM pictures reveal clearly ultrathin hexagonal Pd nanosheets, homogeneous in size with edge lengths of 70−80 nm (Figure 2b,c). We found that the nanosheets are very sensitive to the electron-beam irradiation which creates damage in the samples. TEM pictures taken at low electron-beam intensity show nanosheets of reduced porosity (Figure 2c) whereas strong electron radiation enhances the initial porosity (Figure 2d and Figure S1, Supporting Information). Very few spherical Pd particles were also observed. The selected area electron diffraction (SAED) pattern obtained with a selected aperture of 250 nm of diameter (Figure 2 b, inset) indicates five diffraction rings with a strengthened intensity showing a sixfold symmetry of diffraction. This observation suggests that the nanosheets are single monocrystals which are overlapped and slightly disoriented one with respect to another one. The diffraction rings can be indexed as the (111), (200), (220), (311), and (331) plane lattices. The respective reciprocal distances found as d_1 = 0.223 nm, d_2 = 0.192 nm, d_3 = 0.133 nm, d_4 = 0.117 nm, and d_5 = 0.088 nm are consistent with metal Pd. We note however that the (200) reflection is weak because the

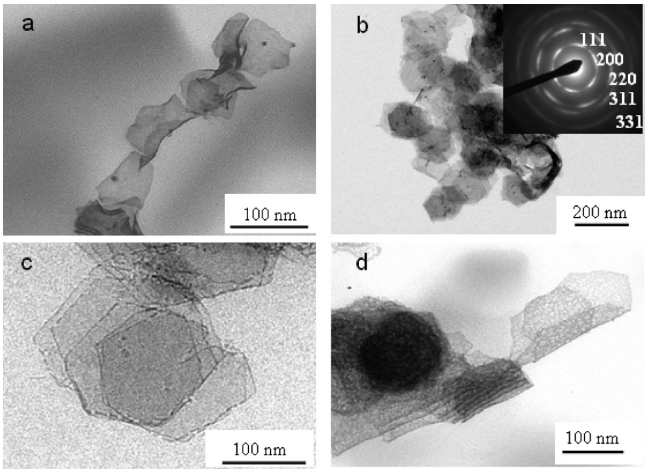

Figure 2. TEM images of palladium nanostructures prepared by the reaction of CO with a Pd complex $Pd_2(DBA)_3$ (a, b, d) or $Pd(OAc)_2$ (c) dissolved in the oil phase of water/toluene/CTAB emulsion. (a) Pd nanosheets after extraction with 2-propanol; (b−d) porous hexagonal nanosheets after washing several times with 2-propanol under ultrasounds; (part b inset) the corresponding SAED.

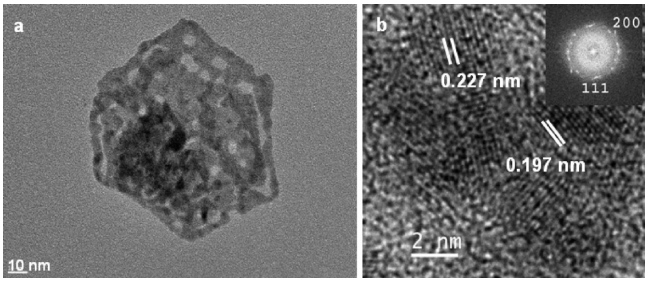

Figure 3. (a) HRTEM images of a single ultrathin hexagonal Pd nanosheets and (b) further magnified image of a selected area on the thin film shown in (a). The FFT (b inset) allows one to measure the two expected reciprocal distances and confirms the structure of cubic Pd.

hexagonal nanosheets are mainly oriented parallel to the supporting substrate.

High resolution TEM (HRTEM) imaging (Figure 3) revealed that the nanosheets obtained from the CTAB-based emulsions or mesophases are porous (with a typical pore size of a few nanometers). The relatively high electron-beam intensity of the instrument setup used for high resolution results in more damage and hence leads to an increase of the porosity of the nanosheets. In addition, we believe that the high intensity beam leads to a modification of the single nanocrystal into small crystallized nanodomains (4−7 nm) (Figure 3b). The fast Fourier transformation (FFT) (Figure 3b, inset) exhibits one main diffraction ring and two discrete symmetric points. The reciprocal distances found, d_1 = 0.227 nm and d_2 = 0.197 nm, correspond respectively to the (111) and (200) plane lattices of cubic Pd. Figures 2d and 4a,b show that the nanosheets are very thin (thickness of the order of 2 nm which corresponds to about 10 layers of atoms) and can fold up to form stacks of nanosheets. The FFT (Figure 4b, inset) reveals here two diffraction rings corresponding to the (111) and (200) planes. The last one is more visible than in Figure 3b as the sheets are viewed from their edges. We note that the same Pd nanostructures

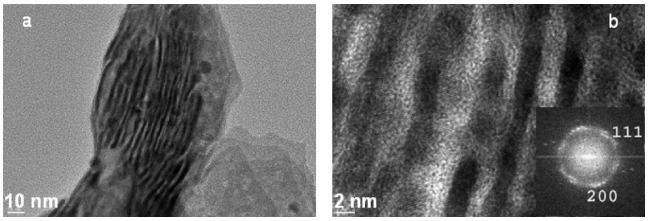

Figure 4. HRTEM images of vertical stacks of hexagonal Pd nanosheets and (b) magnified image of a selected portion of (a) and its corresponding FFT (inset).

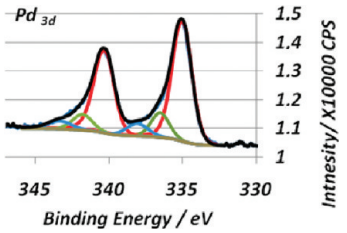

Figure 5. XPS, Pd_{3d} spectrum of Pd nanosheets (formed from a ternary emulsion with CTAB as surfactant and $Pd_2(DBA)_3$ as Pd complex); fit of the Pd 3d region performed using three double-contributions (red, green, and blue lines). The black line is the fit of the experimental data.

were obtained with concentrated and diluted CTAB-based emulsion doped with $Pd_2(DBA)_3$.

X-ray photoelectron spectroscopy (XPS) was performed to confirm the metallic nature of the nanosheets. The XPS analysis showed that the Pd nanosheets exhibit for the Pd_{3d} region two main peaks at 335.8 and 341.0 eV. This double feature is specific to the $3d_{5/2}$ $3d_{3/2}$ spin orbit splitting of the Pd 3d core shell. When position energies are corrected from a slight charge effect systematically observed, the main contributions are then centered at 335.0 and 340.3 eV. The shift is evaluated, using the correction of the C 1s aliphatic component. The fitting procedure presented in Figure 5 shows that a triple double-contribution must be proposed for a good simulation of the global response. The asymmetric shapes of each lowest energy contribution and their positions at 335.0 or 340.3 eV agree with a metallic character of the Pd. Obviously the main XPS response can be associated to pure metallic nanosheets. However, small Pd $3d_{5/2}$ (or Pd $3d_{3/2}$) additional contributions positively shifted by 1.5 and 3.0 eV from the main contribution must be added to achieve a good simulation. This high energy contribution can be interpreted as resulting from a thin oxide contribution (PdO or PdO_2) or a coverage by CO. However, the ratio ($Pd_{tot}/Pd(0) \approx 1.3$) of different contributions shows that the Pd(0) is always the main contribution which is consistent with an assignment of metallic Pd.

The Pd nanosheets exhibit a broad absorption starting from 500 nm to the near-infrared region (Figure 6). Such a broad absorption with highest absorbance in the infrared was previously reported for Pd nanoplates and nanoflowers.[20] It has been shown that Pd nanodisks exhibited broad localized surface plasmons with higher sensitivity of the plasmon to the disk ratio compared to Ag.[26]

(26) Langhammer, C.; Yuan, Z.; Zoric, I.; Kasemo, B. *Nano Lett.* **2006**, *6*, 833.

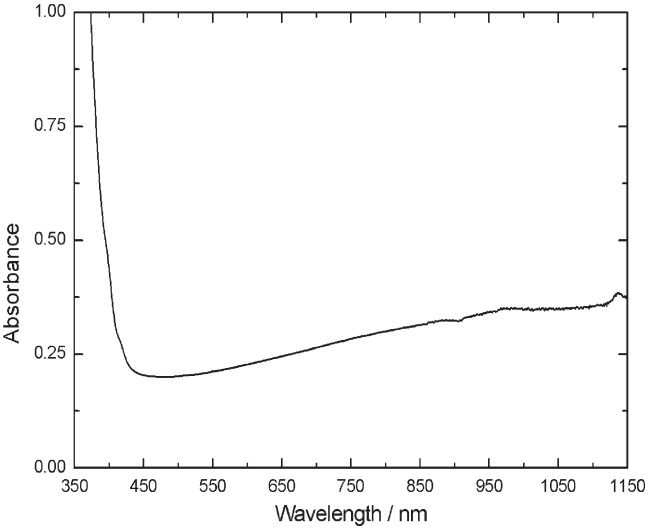

Figure 6. UV−visible spectrum of Pd nanosheets (formed in a CTAB-based mesophase doped with $Pd_2(DBA)_3$) after extraction in 2-propanol.

Xia et al. reported a broad peak at 530 nm for Pd nanoplates of 5 nm thickness.[13] The broadness of the peak has been attributed to the dielectric function of Pd and to the thickness of the plates. The Pd nanosheets in the present study have a much broader peak than the Pd nanodisks or nanoplates presumably because the present nanosheets are thinner (2 nm). Such two-dimensional palladium nanostructures are known to have interesting optical properties that can be exploited for application in optical sensing, SERS, and photothermal heating.[13]

The suspensions of the nanosheets were still blue after 5 months in 2-propanol and exhibited a UV−visible spectrum similar to that of a freshly prepared sample. TEM observations showed mainly 2D-well crystallized nanostructures, but the hexagonal shape was no more conserved (Figure 7). A few 1D nanostructures were also observed. The indexation of the SAED (Figure 7, inset) demonstrates the conservation of the metallic state of Pd.

To understand what the key factors that govern the formation of the Pd nanofilms are, we have changed various parameters such as the Pd precursor and its concentration, the nature of the surfactant, and the reducing agent.

Two other toluene soluble Pd^{II} complexes, namely, $Pd(OAc)_2$ and $Pd(acac)_2$, were therefore used as Pd precursors. Hexagonal mesophases made of water, CTAB as surfactant, pentanol as cosurfactant, and toluene containing $Pd^{II}(OAc)_2$ or $Pd^{II}(acac)_2$ (1.5×10^{-3} M) were treated with CO (1 atm) for a slow reduction of Pd. Similarly to our observation with $Pd_2(DBA)_3$, the color of the mesophases containing $Pd^{II}(OAc)_2$ or $Pd^{II}(acac)_2$ changed from yellow orange into the typical blue color of Pd nanosheets on reaction with CO (Figure 1). The alcoholic solutions on extraction were blue as well, and the absorption spectra of both samples displayed a typical absorption pattern similar to Pd nanosheets obtained from the CTAB-based emulsions and mesophases doped with $Pd_2(DBA)_3$. TEM images of both samples (Figure 2c) showed porous hexagonal nanosheets similar to those obtained previously with $Pd_2(DBA)_3$ (Figure 2a,b,d).

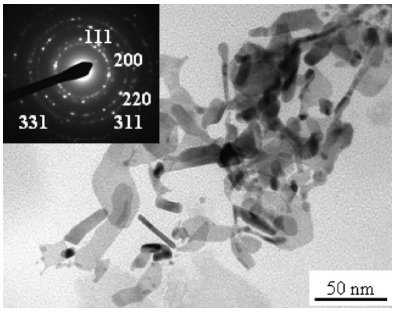

Figure 7. TEM image and SAED (inset) of palladium nanosheets (formed in a CTAB-based mesophase doped with $Pd_2(DBA)_3$) extracted, washed with 2-propanol, and then kept 5 months in suspension in the same solvent.

Thus, the nature of the Pd precursor and the ligands (originating from the precursor) does not seem to influence the morphology of the Pd nanosheets formed in CTAB-based samples. The valency of Pd in its precursor also does not affect the nanosheet formation as we obtained hexagonal Pd nanosheets from $Pd_2(DBA)_3$, where Pd is in zero valency state, and $Pd(OAc)_2$ and $Pd(acac)_2$, where the valency of Pd is II. The effect of the Pd precursor concentration was also investigated. Similar Pd nanosheets were also obtained at higher $Pd(OAc)_2$ (10^{-2} M) concentration.

Experiments with $Pd_2(DBA)_3$ were also conducted in ternary emulsions and hexagonal mesophases based on another surfactant, SDS. After completion of the reaction with CO, the initially wine-red emulsions and mesophases were black in color. The Pd nanomaterials after extraction with 2-propanol did not exhibit absorption in the visible and near-infrared region. In that case, TEM observations showed small elongated Pd nanoparticles and fractals, for the synthesis performed in SDS-based emulsions, or spherical Pd nanoparticles of 2−3 nm for the synthesis performed in SDS-based mesophases (Figure 8). The SAED (Figure 8 b, inset) indicates five diffraction rings. Their respective reciprocal distances are consistent with metal-bonded polycrystalline Pd.

Experiments have been conducted on the doped mesophases using hydrazine as reducting agent instead of CO. In this case also, the reduction is very slow, but different morphologies were obtained: palladium nanowires were synthesized using CTAB-based mesophases as templates while spherical nanoparticles were formed in SDS-based mesophases.[27]

It has to be noted that Franzen et al. have reported that $Pd_2(DBA)_3$ crystallizes at THF/water interfaces forming large nonmetallic hexagonal platelets of a few micrometers (or rods depending on the THF/water ratio).[28,29] In the absence of reducing agent $Pd_2(DBA)_3$ does not react rapidly to form Pd nanoparticles. There is a structural similarity of our hexagonal Pd nanosheets on

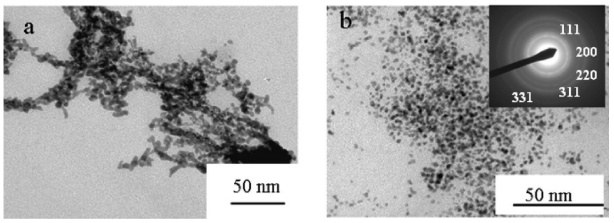

Figure 8. TEM images of palladium nanoparticles prepared by the reaction of CO with $Pd_2(DBA)_3$ (a) in a SDS-based emulsion and (b) in a SDS-based hexagonal mesophase.

the 10−100 nm length scale formed by reduction and hexagonal $Pd_2(DBA)_3$ molecular crystals formed on the 500 nm−10 μm length scale by aggregation. However, in contrast with their findings, our results show that the hexagonal nanosheets (formed by reaction with CO) are composed of metallic palladium. In line with our results, we note that Chaudret et al. have prepared spherical Pd nanoparticles from the same precursor $Pd_2(DBA)_3$ in organic solvents in presence and absence of polymers such as PVP, various cellulose derivatives, hexadecylamine, carbonyl, and phosphine ligands by the reaction with CO.[30]

A plausible process for the role of CO is that it would displace the DBA ligand,[31] leading to the formation of an unstable Pd carbonyl complex, which collapses into metal clusters.[30] The clusters can then aggregate on the CTAB interface forming Pd nanosheets. To confirm that CO can displace the DBA ligand, we have calculated the free enthalpy ΔG of the reaction:

$$Pd_2(DBA)_3 + 4CO \rightarrow Pd_2(CO)_4 + 3DBA \qquad (1)$$

We have used the DFT (density functional theory) with the PBE (Perdew, Burke, Ernzerhof) functional and the SDD (Stuttgart-Dresden) Gaussian basis set as provided by the Gaussian package.[32] The PBE functional yields a value of 1.36 eV for the Pd_2 binding energy, a numerical

(27) Siril, P. F.; Ramos, L.; Beaunier, P.; Prouzet, E.; Remita, H. To be submitted.
(28) Franzen, S.; Cerruti, M.; Leonard, D. N.; Duscher, G. *J. Am. Chem. Soc.* **2007**, *129*, 5340.
(29) Leonard, D. N.; Cerruti, M.; Duscher, G.; Franzen, S. *Langmuir* **2008**, *24*, 7803.
(30) (a) Bradley, J. S.; Hill, E. W.; Behal, S.; Klein, C.; Chaudret, B.; Duteil, A. *Chem. Mater.* **1992**, *4*, 1234. (b) Duteil, A.; Queau, R.; Chaudret, B. *Chem. Mater.* **1993**, *5*, 341. (c) Amiens, C.; Caro, D.; Chaudret, B. *J. Am. Chem. Soc.* **1993**, *115*, 11638. (d) Ramirez, E.; Jansat, S.; Philippot, K.; Lecante, P.; Gomez, M.; Masdeu-Bulto, A. M.; Chaudret, B. *J. Organomet. Chem.* **2004**, *689*, 4601.
(31) Belli Dell' Amico, D.; Calderazzo, F.; Dittmann, M.; Labella, L.; Marchetti, F.; Schweda, E.; Strähle, J. *J. Organomet. Chem.* **1999**, *583*, 162.
(32) Frisch, M. J.; Trucks, G. W.; Schlegel, H. B.; Scuseria, G. E.; Robb, M. A.; Cheeseman, J. R.; Montgomery, J. A.; Vreven, T., Jr.; Kudin, K. N.; Burant, J. C.; Millam, J. M.; Iyengar, S. S.; Tomasi, J.; Barone, V.; Mennucci, B.; Cossi, M.; Scalmani, G.; Rega, N.; Petersson, G. A.; Nakatsuji, H.; Hada, M.; Ehara, M.; Toyota, K.; Fukuda, R.; Hasegawa, J.; Ishida, M.; Nakajima, T.; Honda, Y.; Kitao, O.; Nakai, H.; Klene, M.; Li, X.; Knox, J. E.; Hratchian, H. P.; Cross, J. B.;Adamo, C.; Jaramillo, J.; Gomperts, R.; Stratmann, R. E.; Yazyev, O.; Austin, A. J.; Cammi, R.; Pomelli, C.; Ochterski, J. W.; Ayala, P. Y.; Morokuma, K.; Voth, G. A.; Salvador, P.; Dannenberg, J. J.; Zakrzewski, V. G.; Dapprich, S.; Daniels, A. D.; Strain, M. C.; Farkas, O.; Malick, D. K.; Rabuck, A. D.; Raghavachari, K.; Foresman, J. B.; Ortiz, J. V.; Cui, Q.; Baboul, A. G.; Clifford, S.; Cioslowski, J.; Stefanov, B. B.; Liu, G.; Liashenko, A.; Piskorz, P.; Komaromi, I.; Martin, R. L.; Fox, D. J.; Keith, T.; Al-Laham, M. A.; Peng, C. Y.; Nanayakkara, A.; Challacombe, M.; Gill, P. M. W.; Johnson, B.; Chen, W.; Wong, M. W.; Gonzalez, C.; Pople, J. A. *Gaussian 03*, Revision C.02; Gaussian Inc.: Wallingford, CT, **2004**.

value very close to the relativistic value (1.39 eV),[33] and a value of 2.46 eV for the Pd−CO binding energy. This latter numerical value is overestimated, the relativistic value being equal to 2.10 eV.[34] We have obtained for the free enthalpy of reaction 1 the crude PBE value $\Delta G = -1.82$ eV, which must be corrected by the error on four Pd−CO bonds ($(2.36-2.10) \times 4 = 1.44$ eV). This yields the corrected PBE value: $\Delta G = -0.38$ eV, which shows that four CO could displace efficiently the three DBA ligands. This calculation could help understanding the primary steps for synthesis of Pd nanosheets starting from $Pd_2(DBA)_3$.

On the other hand, the reduction mechanisms of Pd^{II} complexes by CO are not known but imply formation of Pd carbonyl complexes and clusters.[35] Note that CO alone cannot stabilize Pd clusters, and pure carbonyl Pd clusters were only observed in zeolites.[36]

The reaction of $Pd_2(DBA)_3$ with CO is very fast in toluene solution, and we obtained only large black Pd particles that settle at the bottom of the vial instantaneously when the reaction was carried out without using stabilizers other than CO (data not shown). By contrast, the reaction in the emulsions and mesophases lead to spherical or elongated particles with SDS as surfactant and to hexagonal Pd nanosheets with CTAB-based samples. Regulating the kinetics of nucleation and the particle growth was also identified as a key factor in obtaining 2D Pd nanostructures in previous studies.[13,20] The slow diffusion of CO in the emulsions and mesophases followed by a slow reduction or ligandation by CO are presumably the key factors responsible for the formation of Pd nanosheets because it involves a slow nucleation of metallic particles. Our experiments show that CO plays an important role in defining the morphology of the nanosheets and intermediate unstable palladium carbonyl clusters are probably involved in the nucleation/growth process.

We have proved that the presence of a complexing agent such as CTAB is also essential for the formation of hexagonal nanosheets from emulsion and mesophase, as experiments performed with SDS-based samples lead only to nanoparticles (Figure 8). This is presumably due to specific interactions of CTAB with the Pd precursors. Indeed, while solutions of the Pd-precursor ($Pd_2(DBA)_3$) in toluene are red as the SDS-based samples containing the precursors, samples with CTAB are systematically orange. UV−visible absorption spectra show that the $Pd(DBA)_2$ solution exhibits an absorption maximum at 520 nm. This peak is also observed for SDS-based samples while it is not present in the case of CTAB-based mesophases, comforting the fact that CTAB complexes the $Pd_2(DBA)_3$. In addition, we expect that, during the growth process, CTAB could also adsorb to certain crystal faces promoting specific crystal growth.

It has to be noted that the reduction of $Pd(OAc)_2$ by CO in toluene solutions of highly branched amphiphilic polymers leads to quite similar Pd hexagonal nanoplates.[37] In this study, the authors have also identified the essential role of CO as well as the importance of the interaction of the Pd with the polar scaffold of the polymer for the formation of the nanoplates. 2D nanostructures (hexagons and other shapes) were also recently obtained by photoreduction of $Pd(acac)_2$ in 2-propanol under CO atmosphere.[20] In this case also the slow reduction in the presence of CO was found to be essential for obtaining these 2D morphologies.

Thus, local nucleation, slow growth because of slow reaction with CO limited by its diffusion followed by ligandation by CO, and complexation/adsorption of CTAB seem to be the key factors responsible for the formation of Pd nanosheets. The parameters that control the characteristic size (thickness and edge length) of the hexagonal nanosheets remain however to be elucidated.

IV. Conclusion

Hexagonal, thin palladium nanosheets were synthesized in emulsions formed by a ternary system (water, toluene containing Pd complexes, CTAB as surfactant) and in quaternary hexagonal mesophases formed by water, toluene containing Pd complexes, CTAB, and a cosurfactant. These nanostructures are formed by slow ligand exchange or reduction (depending on the Pd precursor) and nucleation provided by CO on the CTAB interface. The thin Pd nanosheets exhibit a broad absorption band from the visible to the near-infrared region. Their optical properties may render them useful for application in optical sensing and photothermal heating. These nanostructures may also find application in catalysis and electrocatalysis. Moreover, it has to be noted that the present nanosheets are ultrathin and porous and hence have larger surface area so that they can be more efficient in hydrogen storage and catalysis than the nonporous films. The present nanosheets exhibit sharp corners and edges, and hence they may serve as active substrates for surface enhanced Raman scattering (SERS).

Acknowledgment. P.F.S. acknowledges the European Commission for a postdoctoral fellowship (MIF1-CT-2006-021579). The authors thank Stefan Franzen (North Carolina State University) for helpful discussion and Jackie Vigneron (Institut Lavoisier, Université Versailles Saint Quentin-en-Yvelines) for his assistance for XPS experiments.

Supporting Information Available: Additional TEM picture (PDF). This material is available free of charge via the Internet at http://pubs.acs.org.

(33) Xiao, C.; Krüger, S.; Belling, T.; Mayer, M.; Rösch, N. *Int. J. Quantum Chem.* **1999**, *74*, 405.
(34) Chung, S. C .; Krüger, S.; Pacchioni, G.; Rösch, N. *J. Chem. Phys.* **1995**, *102*, 3695.
(35) Shim, I.-W.; Kim, D.-Y.; Choi, S.; Kong, K.-H.; Choe, J.-I. *React. Funct. Polym.* **2000**, *43*, 287.
(36) Sheu, L.- L.; Knözinger, H.; Sachtler, W. M. H. *J. Am. Chem. Soc.* **1989**, *111*, 8125.
(37) Schlotterbeck, U.; Aymonier, C.; Thomann, R.; Hofmeister, H.; Tromp, M.; Richtering, W.; Mecking, S. *Adv. Funct. Mater.* **2004**, *14*, 999.